

# $^{10}\text{B}$ Concentration, Phantom Size and Tumor Location Dependent Dose Enhancement and Neutron Spectra in Boron Neutron Capture Therapy

Izadi Vasafi Gh.<sup>1\*</sup>, Firoozabadi M. M.<sup>1</sup>

## ABSTRACT

**Background:** The amount of average dose enhancement in tumor loaded with  $^{10}\text{B}$  may vary due to various factors in boron neutron capture therapy.

**Objective:** This study aims to evaluate dose enhancement in tumor loaded with  $^{10}\text{B}$  under influence of various factors and investigate the dependence of this dose enhancement on neutron spectra changes.

**Material and Methods:** In this simulation study, using  $^{252}\text{Cf}$  as a neutron source, the average in-tumor dose enhancement factor (DEF) and neutron energy spectra were calculated for various  $^{10}\text{B}$  concentrations, phantom with different sizes and for different tumor locations, through MCNPX code.

**Results:** Obtained results showed that the values of average DEF rise with increasing  $^{10}\text{B}$  concentration, phantom diameter (< 30 cm) and tumor distance from the source, but this increment is not linear.

**Conclusion:** It was concluded that inequality in average dose enhancement rates, in tumor loaded with  $^{10}\text{B}$  under influence of various factors in boron neutron capture therapy, is due to non-identical changes of both the thermal neutron flux with increasing same number of  $^{10}\text{B}$  atoms and same thickness of scattering material, and the thermal to fast neutron flux ratio with increasing equal distances of tumor from the source.

**Citation:** Izadi Vasafi Gh, Firoozabadi M. M.  $^{10}\text{B}$  Concentration, Phantom Size and Tumor Location Dependent Dose Enhancement and Neutron Spectra in Boron Neutron Capture Therapy. *J Biomed Phys Eng.* 2019;9(6):653-660. <https://doi.org/10.31661/jbpe.v0i0.799>.

## Keywords

Boron neutron Capture Therapy; Dose Enhancement; Neutrons; Monte Carlo Method

## Introduction

One of the methods used for cancer treatment, especially brain tumors (glioblastomas) and skin cancer (melanomas), is neutron capture therapy (NCT). The physical principle of NCT is based on the nuclear reaction occurring when a stable isotope is irradiated with thermal neutrons to yield highly energetic particles [1]. The  $^{10}\text{B}$  isotope is the most suitable agent in NCT as it possesses high cross-section for thermal neutron capture (3838 barns) and also is not toxic. Following the neutron capture, the excited boron-11 ( $^{11}\text{B}^*$ ) is produced, which decays into high linear energy transfer (LET) alpha particles and lithium nucleus. These high energy particles have short path lengths in biologi-

<sup>1</sup>PhD, Department of Physics, Faculty of Sciences, University of Birjand, Birjand, Iran

\*Corresponding author:  
Gh. Izadi Vasafi  
Department of Physics,  
Faculty of Sciences,  
University of Birjand,  
Birjand, Iran  
E-mail: ghizadivasafi@  
birjand.ac.ir

Received: 20 May 2017  
Accepted: 23 July 2017

cal tissue (5-9  $\mu\text{m}$ ) which confine the radiation damage to the cell containing the  $^{10}\text{B}$  nuclide. Clinical application of boron neutron capture therapy (BNCT) includes the treatment of brain tumors, melanoma, head and neck cancer, colorectal cancer and liver cancer [2,3].

Various sources can be used as a neutron source in neutron capture therapy such as reactors, accelerator-based and  $^{252}\text{Cf}$  sources. Most reactors are far from hospitals and their use for clinical NCT is difficult; thus, other neutron sources, such as accelerator-based and  $^{252}\text{Cf}$ , have been suggested for NCT [4]. There are some studies that  $^{252}\text{Cf}$  was applied as a neutron source for use in NCT [5,6].

In neutron interaction with matter, reduction of neutron energy to the thermal energy range due to multiple scatterings and thus increasing the probability of thermal neutron capture by  $^{10}\text{B}$  cause dose enhancement in tumor loaded with  $^{10}\text{B}$  in BNCT [7,8]. The amount of average dose enhancement in tumor may vary owing to influence of various factors. The purpose of this study is to evaluate dose enhancement in tumor loaded with  $^{10}\text{B}$  under influence of various factors and investigate the dependence of this enhancement on neutron energy spectra in BNCT.

Herein, the use of  $^{252}\text{Cf}$  as a neutron source and calculations of dose enhancement in tumor loaded with  $^{10}\text{B}$  were made for various concentrations of  $^{10}\text{B}$ , phantom with different sizes and for different locations of tumor in phantom, through Monte Carlo simulation. Moreover, the neutron spectra of  $^{252}\text{Cf}$  source were examined as a function of  $^{10}\text{B}$  concentration, phantom diameter and the radial distance of tumor from the source to investigate the dependence of dose enhancement in tumor under influence of these factors on neutron spectra changes.

## Material and Methods

### The simulated source geometry

In this simulation study, a  $^{252}\text{Cf}$  applicator

tube (AT) source was used as a neutron source [9]. The source was composed of a cylindrical active core, primary and secondary capsules. The cylindrical active core was made of californium oxide,  $\text{Cf}_2\text{O}_3$ , with  $12\text{ g/cm}^3$  density. The radius and length of the active core was 0.615 and 15 mm, respectively. This active cylinder was located in a primary capsule of Pt/Ir-10% mass, with the inner and outer diameters of 1.35 and 1.75 mm, and the inner and outer lengths of 15.50 and 17.78 mm, respectively. The secondary capsule had the inner and outer diameters of 1.80 and 2.80 mm, and inner and outer lengths of 17.82 and 23.14 mm, respectively. The ends of the primary and secondary capsules were welded and rounded. In addition, a bodkin eyelet with 0.635 mm diameter was also embedded in the secondary capsule of the source. Figure 1 shows a general description of the  $^{252}\text{Cf}$  AT source simulated in this study.

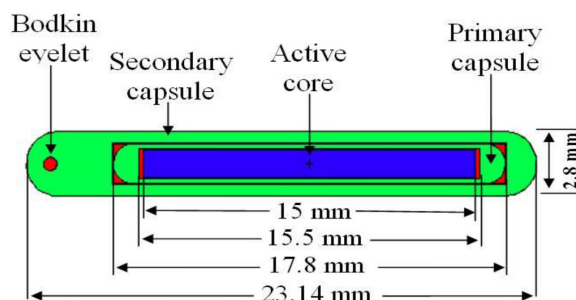


**Figure 1:** Geometry of the simulated  $^{252}\text{Cf}$  AT source

### Dose enhancement calculations

The  $^{252}\text{Cf}$  AT source was positioned at the center of a spherical phantom filled with water of  $0.998\text{ g/cm}^3$  density. A volume with the dimensions of  $2\text{ cm} \times 2\text{ cm} \times 2\text{ cm}$  along the transverse axis from the source center was assumed as a tumor.

For the evaluation of dose enhancement in tumor loaded with  $^{10}\text{B}$ , the concept of dose enhancement factor (DEF), which is defined as the ratio of the total dose in a voxel containing

$^{10}\text{B}$ , to the total dose in the same voxel without the presence of  $^{10}\text{B}$  was used. The  $^{10}\text{B}$  was assumed to be uniformly distributed throughout the tumor volume mixing the water. The total dose is the sum of dose contributions from the neutrons and gamma-rays emitted from the source, induced gamma rays as a result of capture of thermal neutrons by hydrogen and boron due to the capture of thermal neutrons by  $^{10}\text{B}$ ,  $^{10}\text{B}(n, \alpha)$ ,  $^7\text{Li}$ .

To evaluate dose enhancement at various points inside the tumor volume loaded with  $^{10}\text{B}$  and determine the impact of various concentrations of  $^{10}\text{B}$  on dose enhancement, at first, the total dose inside various voxels of the tumor (along the transverse axis of the source), was calculated before and after the tumor, in the case that  $^{10}\text{B}$  did not exist in the tumor. Then this process was performed for the same tumor, but loaded with 100-500 ppm  $^{10}\text{B}$  and the corresponding values of DEF in the voxels were calculated. The tumor was positioned at a distance of 1 cm from the source center and the diameter of the phantom was 30 cm.

In addition to the  $^{10}\text{B}$  concentration, the average in-tumor dose enhancement factor, which is the average of the values of dose enhancement factors in tumor (along the transverse axis from the source center) was calculated in separate simulations to evaluate the impact of phantom size and tumor location on dose enhancement. Firstly, the average DEF was calculated in tumor loaded with 100 ppm  $^{10}\text{B}$ , which was located at a distance of 1 cm from the source center in phantom of varying diameters ranging from 10 to 50 cm. Secondly, the average DEF was calculated for tumor, which was located at different distances, including 1, 3, 5, 7 and 9 cm along the transverse axis from the source center. In this case, the tumor was loaded with 100 ppm  $^{10}\text{B}$  and the diameter of the phantom was 30 cm. Then, the  $^{252}\text{Cf}$  neutron spectra of at each  $^{10}\text{B}$  concentration, phantom diameter and the radial distance of the tumor from the source were calculated, separately.

### Monte Carlo simulation

In the present study, MCNPX code (version 2.6.0) [10] was used to calculate dose. The neutron dose was calculated using the fluence-to-kerma conversion factors for water [11]. The energy deposited by both the source and induced gamma rays was obtained using the \*F8 tally. The \*F8 tally output (MeV) in each tally cell was divided by the mass of that cell to convert the energy deposited into dose (MeV/g). The boron dose was estimated using the calculation of kerma factors for  $^{10}\text{B}$  [12]. The dose rate was determined in a cylindrical annulus with 0.2 cm thickness and 0.2 cm depth positioned in the tumor, before and after it along the transverse axis from the source center; in addition, the neutron energy spectrum of the  $^{252}\text{Cf}$  source was modeled as a watt fission spectrum. The photon spectrum of the  $^{252}\text{Cf}$  source was obtained from Stoddard and Hootman [13]. A number of  $10^8$  and  $10^9$  neutrons and photons, respectively, were run in each input file. Energy cut off for electrons and photons in all input files was set as 10 keV. The solid state  $S(\alpha, \beta)$  neutron scattering library (lwtr.01t) was used in order to improve the accuracy of low energy neutron transport calculations. The relative error of calculations was lower than 2%.

### Results

To validate the Monte Carlo simulation, the total dose computed in this study was compared with the experimental and simulated values, which were published in the literature. Figure 2 shows a comparison between our simulated total dose rates with the experimental measurements of Colvett et al., [14] and the simulated calculations of Krishnaswamy [15]. There is a good agreement between the values with small discrepancies at short distances to the source. These discrepancies are attributed to the different modeled neutron and photon energy spectra of the  $^{252}\text{Cf}$  source in the simulations or the spatial precision and sensitivity of measurement devices to rapid change of ra-

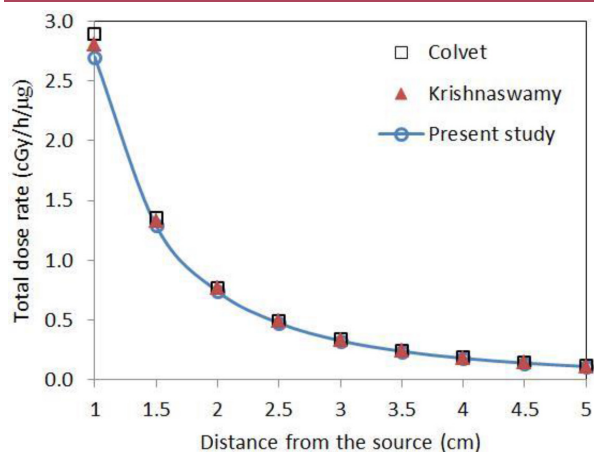


**Figure 2:** Calculated and measured total dose rates for a water phantom.

diation dose.

After validation, the validated computer code was applied for calculation of total dose and neutron energy spectra. Figures 3a, b and c shows the total dose rates calculated at various points inside the tumor volume for various concentrations of  $^{10}\text{B}$ , different phantom sizes and different distances of the tumor from the source. This figure indicates that the values of total dose rose with increasing  $^{10}\text{B}$  concentration and phantom diameter, but reduced with increasing tumor distance from the source. The differences between dose enhancement rates by increasing the amounts of various factors, especially  $^{10}\text{B}$  concentration or phantom diameter are not evident in the graph. The dose enhancement factor in tumor loaded with  $^{10}\text{B}$  was calculated under the influence of various factors in order to highlight any discrepancy between dose enhancements in tumor under influence of these factors.

Figure 4 shows the changes of dose enhancement factors at various points inside tumor volume loaded with 100-500 ppm  $^{10}\text{B}$ , before and after tumor. As is seen, the value of DEF increased gradually in tumor volume with increasing distance inside the tumor and reached its highest value at the end of the tumor. The values of average DEF also rose with increasing concentration of  $^{10}\text{B}$ . The values of average DEF were estimated 1.10, 1.25 and 1.37

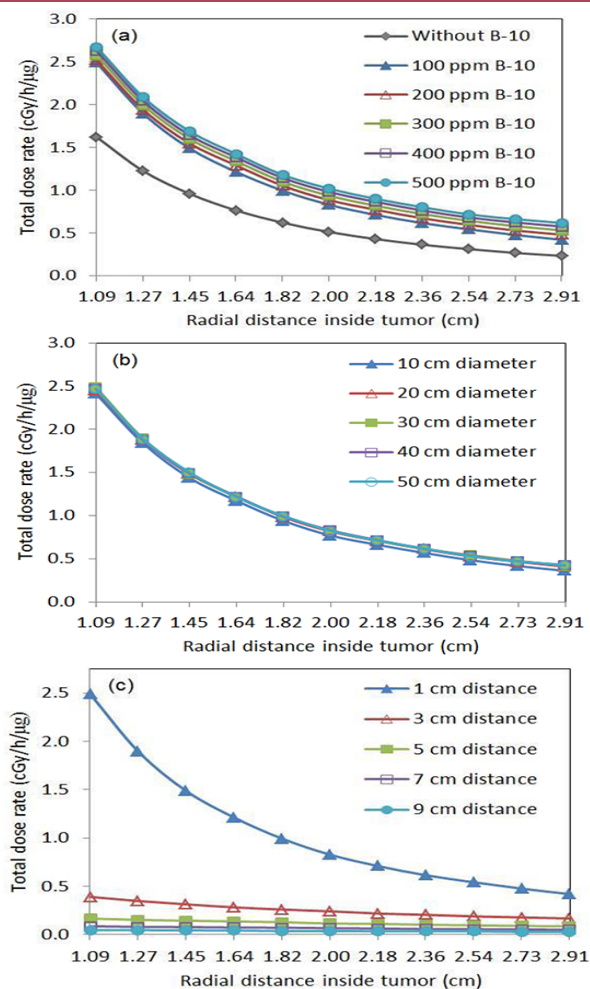


**Figure 3:** Total dose rate distributions in the tumor: (a) for various  $^{10}\text{B}$  concentrations; (b) located in a phantom of different diameters; (c) at different distances from the source

for concentrations of 100, 300 and 500 ppm  $^{10}\text{B}$ , respectively. In all cases, the existence of  $^{10}\text{B}$  inside the tumor has not changed the values of DEF noticeably at distances before the tumor region, but the values of DEF decreased slightly at distances after tumor because of the  $^{10}\text{B}$  shielding effect.

Figures 5a and b shows how dose enhancement in tumor depends on the size of phantom and tumor location. It is seen that the values of average DEF rise with increasing phantom diameter and tumor distance from the source. It is also visible that the values of average DEF do not rise linearly with increasing phantom

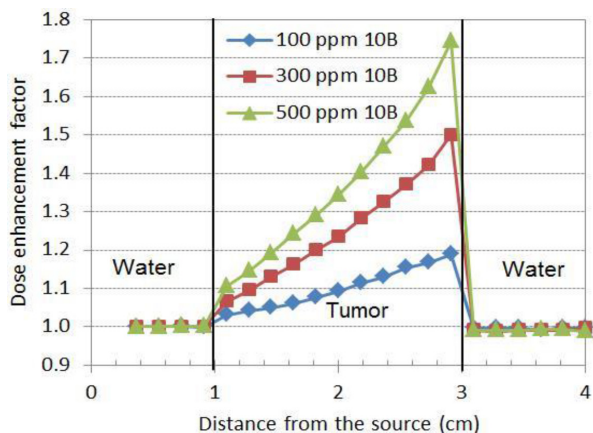


**Figure 4:** DEF calculated in tumor loaded with different  $^{10}\text{B}$  concentrations located at a distance of 1 cm from the source center in a 30 cm diameter phantom.

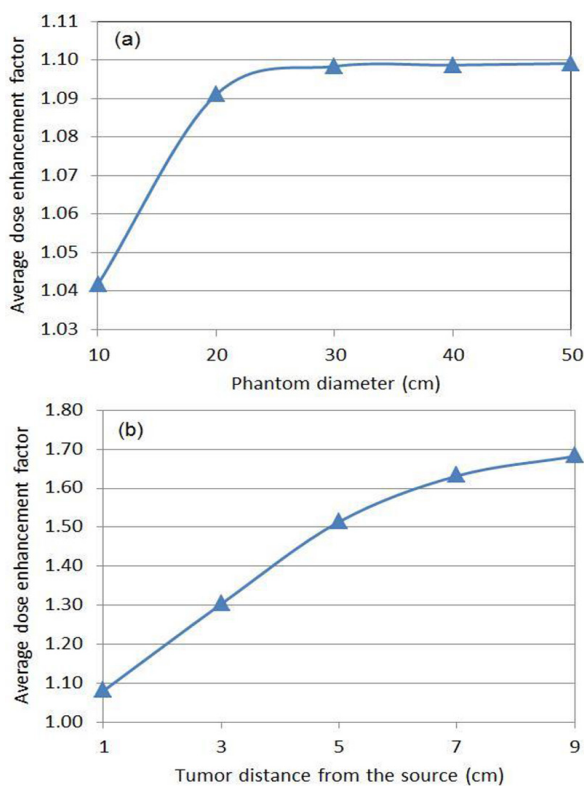


**Figure 5:** Calculated average DEF in the tumor: (a) located at a distance of 1 cm from the source center in a phantom of varying diameters; (b) located at different distances from the source center in a 30 cm diameter phantom

diameter and tumor distance from the source. The average DEF increased 4.73% from 1.045 to 1.097 for phantoms of 10 and 20 cm diameter, respectively, with a 5.43% increase from 1.045 to 1.105 for phantoms of 10 and 30 cm diameter, respectively. Increasing the thickness of scattering material has increased the value of average DEF. The increment of average DEF is up to the diameter of 30 cm and after that, the average DEF becomes uniform as is seen in Figure 6a. The enhancement rate

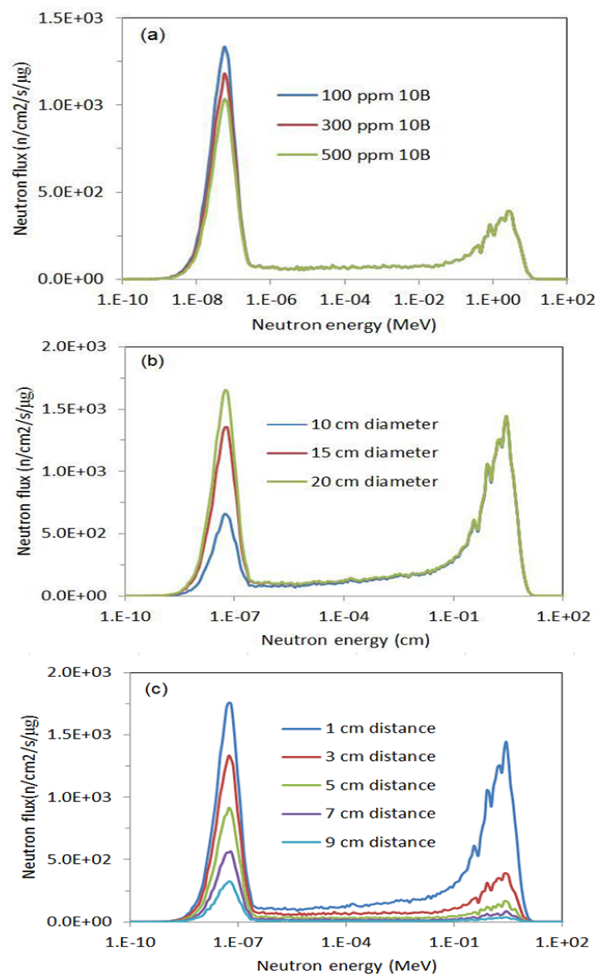


**Figure 6:** Calculated neutron energy spectra of  $^{252}\text{Cf}$  in the tumor: (a) loaded with various concentrations of 100, 300 and 500 ppm  $^{10}\text{B}$  (from top to bottom); (b) located in a phantom of 10, 15 and 20 cm diameters (from bottom to top); (c) located at distances of 1, 3, 5, 7 and 9 cm from the source center (from top to bottom).

of average DEF is 16.17% from 1.30 to 1.51 for tumors located at distances of 3 and 5 cm from the source, respectively, while it is 7.76% from 1.51 to 1.63 for tumors located at distances of 5 and 7 cm from the source, respectively. Therefore, the enhancement proportion of average DEF is higher at shorter distances of the tumor from the source.

Figures 6a, b and c illustrate the changes of  $^{252}\text{Cf}$  neutron energy spectra calculated for various  $^{10}\text{B}$  concentrations, different phantom sizes and different distances of the tumor from

the source. It is visible that in all cases that there is a significant change in the thermal neutron flux under influence of these factors. The fast neutron flux has just changed with increasing tumor distance from the source.

The amounts of both the thermal neutron flux and the thermal to fast neutron flux ratio for different concentrations of  $^{10}\text{B}$ , phantom diameter and tumor location are presented in Table 1. We noticed that the thermal neutron flux has not changed equally with increasing the same concentrations of  $^{10}\text{B}$  and same

**Table 1:** Thermal neutron flux and thermal to fast neutron flux ratio for various concentrations of  $^{10}\text{B}$ , a variety of phantom diameters and different distances of tumor from the source.

$^{10}\text{B}$ concentration (ppm)	Thermal neutron flux (n/cm <sup>2</sup> .s.μg)	Phantom diameter (cm)	Thermal neutron flux (n/cm <sup>2</sup> .s.μg)	Tumor distance (cm)	Thermal to fast neutron flux ratio
100	18595.24	10	9504.68	1	0.85
300	16271.34	15	19064.83	5	3.50
500	14337.61	20	23044.60	9	5.09

diameters of phantom, and also the thermal to fast neutron flux ratio with increasing equal distances of tumor from the source.

## Discussion

Figure 4 indicates that the presence of  $^{10}\text{B}$  inside tumor volume causes the amount dose enhancement in tumor to rise with increasing radial distance inside tumor volume and concentration of  $^{10}\text{B}$ . Indeed, in boron neutron capture therapy, various points inside tumor volume loaded with  $^{10}\text{B}$  will experience different dose enhancements despite the uniform distribution of  $^{10}\text{B}$  throughout tumor volume. With increasing  $^{10}\text{B}$  concentration or in other words, with increasing the number of atoms contributing to the thermal neutron capture reactions, the thermal neutron flux will decrease as is seen in Figure 6a. Therefore, with increasing  $^{10}\text{B}$  concentration and subsequently increasing the number BNC reactions resulting in the increase of the BNC dose rate, the values of average DEF will increase.

With increasing the phantom diameter, in other words, with increasing the thickness of scattering material, the thermal neutron flux increases, as is seen in Figure 6b. Therefore, with increasing phantom diameter, and as a result, increasing the probability of  $^{10}\text{B}$  thermal neutron capture reactions and subsequently increasing the BNC dose rate, the values of average DEF increased in Figure 5a. Because of non-identical increment of thermal neutron flux with increasing the phantom diameter that is apparent from Figure 6b and Table 1, the enhancement proportion of average DEF decreased with increasing phantom diameter.

With increasing tumor distance from the source and decreasing the fast neutron energy due to multiple scatterings, the ratio of thermal to fast neutrons increases (Figure 6c) which results in an increase of the values of average DEF with increasing tumor distance from the source, as is seen in Figure 5b. According to Table 1 data, since the difference between the amounts of thermal to fast neutron flux ratio

is more at shorter distances of tumor to the source, the enhancement proportion of average DEF is higher at these distances.

## Conclusion

In this study, MCNPX code was applied to evaluate the impact of  $^{10}\text{B}$  concentration, phantom size and tumor location on dose enhancement in tumor loaded with  $^{10}\text{B}$  and investigate the dependence of this dose enhancement on neutron spectra changes in boron neutron capture therapy. Obtained results showed that the presence of  $^{10}\text{B}$  inside tumor volume in boron neutron capture therapy causes dose the amount of enhancement in tumor to be variable at various points of tumor despite uniform distribution of  $^{10}\text{B}$  throughout tumor volume. The average dose enhancement in tumor loaded with  $^{10}\text{B}$  rises with increasing  $^{10}\text{B}$  concentration, phantom diameter (< 30 cm) and tumor distance from the source. This increment is not equal with increasing same amounts of these factors. It resulted from the non-identical changes of both the thermal neutron flux with increasing same number of  $^{10}\text{B}$  atoms and same thickness of scattering material, and the thermal to fast neutron flux ratio with increasing equal distances of tumor from the source.

## Acknowledgment

The authors are grateful to Birjand University for the financial support of this work.

## Conflict of Interest

None

## References

1. Enger SA, Rezaei A, Munck af Rosenschold P, Lundqvist H. Gadolinium neutron capture brachytherapy (GdNCB), a new treatment method for intravascular brachytherapy. *Med Phys*. 2006;**33**:46-51. doi: 10.1118/1.2146050. PubMed PMID: 16485408.
2. Barth RF, Coderre JA, Vicente MG, Blue TE. Boron neutron capture therapy of cancer: current status and future prospects. *Clin Cancer Res*.

- 2005;**11**:3987-4002. doi: 10.1158/1078-0432.CCR-05-0035. PubMed PMID: 15930333.
3. Miyatake S, Kawabata S, Hiramatsu R, Kuroiwa T, Suzuki M, Kondo N, et al. Boron Neutron Capture Therapy for Malignant Brain Tumors. *Neurol Med Chir (Tokyo)*. 2016;**56**:361-71. doi: 10.2176/nmc.ra.2015-0297. PubMed PMID: 27250576; PubMed PMCID: PMCPMC4945594.
4. Amin Shokr A. Current Status of Neutron Capture Therapy. IAEA-TECDOC-1223. Vienna: International Atomic Energy Agency; 2001.
5. Wierzbicki JG, Maruyama Y, Porter AT. Measurement of augmentation of  $^{252}\text{Cf}$  implant by  $^{10}\text{B}$  and  $^{157}\text{Gd}$  neutron capture. *Med Phys*. 1994;**21**:787-90. doi: 10.1118/1.597324. PubMed PMID: 7935215.
6. Beach JL, Schroy CB, Ashtari M, Harris MR, Maruyama Y. Boron neutron capture enhancement of  $^{252}\text{Cf}$  brachytherapy. *Int J Radiat Oncol Biol Phys*. 1990;**18**:1421-7. doi: 10.1016/0360-3016(90)90317-d. PubMed PMID: 2370192.
7. Carlsson J, Hartman T, Grusell E. Dose enhancement in fast neutron tumour therapy due to neutron captures in  $^{10}\text{B}$ . *Acta Oncol*. 1994;**33**:315-22. doi: 10.3109/02841869409098423. PubMed PMID: 8018361.
8. Krstic D, Jovanovic Z, Markovic V, Nikezic D, Urosevic V. MCNP simulation of the dose distribution in liver cancer treatment for BNC therapy. *Open Physics*. 2014;**12**:714-8. doi: 10.2478/s11534-014-0507-2.
9. Rivard MJ, Wierzbicki JG, Van Den Heuvel F, Martin RC, McMahon RR. Clinical brachytherapy with neutron emitting  $^{252}\text{Cf}$  sources and adherence to AAPM TG-43 dosimetry protocol. *Med Phys*. 1999;**26**:87-96. doi: 10.1118/1.598472. PubMed PMID: 9949403.
10. Pelowitz DB. MCNPX user's manual, version 2.6.0, LA-CP-07-1473. Los Alamos National Laboratory, Los Alamos (NM; 2008.
11. Chadwick MB, Barschall HH, Caswell RS, DeLuca PM, Hale GM, Jones DT, et al. A consistent set of neutron kerma coefficients from thermal to 150 MeV for biologically important materials. *Med Phys*. 1999;**26**:974-91. doi: 10.1118/1.598601. PubMed PMID: 10436900.
12. Goorley JT, Kiger Iii WS, Zamenhof RG. Reference dosimetry calculations for neutron capture therapy with comparison of analytical and voxel models. *Med Phys*. 2002;**29**:145-56. doi:

- 10.1118/1.1428758. PubMed PMID: 11865986.
13. Stoddard DH, Hootman HE. Cf-252 Shielding Guide. Report DP-1246. Savannah River Laboratory; 1971. P. 1-81.
14. Colvett RD, Rossi HH, Krishnaswamy V. Dose distributions around a californium-252 needle. *Phys Med Biol.* 1972;**17**:356-64. doi: 10.1088/0031-9155/17/3/302. PubMed PMID: 5070446.
15. Krishnaswamy V. Calculated depth dose tablets for californium-252 sources in tissue. *Phys Med Biol.* 1972;**17**:56-63. doi: 10.1088/0031-9155/17/1/006. PubMed PMID: 5071502.